Superionic Conductivity Invoked by Enhanced Correlation Migration in Lithium Halides Solid Electrolytes

Rui Li[†1,2], Pushun Lu[†3,4], Xinmiao Liang[†5], Liwei Liu[1,2], Maxim Avdeev[6], Zhi Deng[7], Shuai Li[7], Kaiqi Xu[8], Jiwen Feng[5], Rui Si[1,2], Fan Wu*[3,4,9,10,11], Zhizhen Zhang*[1,2,12], Yong-Sheng Hu*[3,4]

[1] *School of Materials, Shenzhen Campus of Sun Yat-Sen University, Shenzhen, 518107, Guangdong, P. R. China*

[2] *School of Materials, Sun Yat-Sen University, Guangzhou, 510006, P. R. China*

[3] *Beijing Advanced Innovation Center for Materials Genome Engineering, Key Laboratory for Renewable Energy, Beijing Key Laboratory for New Energy Materials and Devices, Institute of Physics, Chinese Academy of Sciences; Beijing, 100190, P. R. China*

[4] *School of Physical Sciences, University of Chinese Academy of Sciences; Beijing, 100190, P. R. China*

[5] *Innovation Academy for Precision Measurement Science and Technology, Wuhan Institute of Physics and Mathematics, Chinese Academy of Sciences, Wuhan, 430071, P. R. China*

[6] *Australian Nuclear Science and Technology Organisation Locked Bag 2001, Kirrawee DC, NSW 2232, Australia*

[7] *Department of Physics and Academy for Advanced Interdisciplinary Studies, Southern University of Science and Technology, Shenzhen, 518055, P. R. China*

[8] *China Southern Power Grid Technology Co. Ltd., Guangzhou, 510080, P. R. China*

[9] *Yangtze River Delta Physics Research Center; Liyang, Jiangsu, 213300, P. R. China*

[10] *Nano Science and Technology Institute, University of Science and Technology of China; Suzhou, 215123, P. R. China*

[11] *CASOL Energy Co Ltd，Liyang, Jiangsu, 213300, China*

[12] *21C Innovation Laboratory, Contemporary Amperex Technology Ltd. (21C LAB), Ningde, Fujian, 352100, P. R. China*

† These authors contribute equally to this work.

Corresponding authors: Z. Zhang (zhangzhzh28@mail.sysu.edu.cn); F. Wu (fwu@iphy.ac.cn); Y.S. Hu (yshu@iphy.ac.cn)

Experimental Section

Material Synthesis. $Li_{3-x}Sc_{1-x}Zr/Hf_xCl_6$ (x = 0, 0.25, 0.50, 0.625, 0.75, 1.0) were synthesized by a solid-state reaction using LiCl, $ScCl_3$ and $ZrCl_4$ or $HfCl_4$. The raw materials were sealed in a 100 ml zirconia jar under inert conditions (argon atmosphere) with zirconia balls (o.d. 3 mm) by applying a sample-to-ball mass ratio of 1:20. The mixture was milled with planetary ball milling (Retsch) for a duration of 10 h over 400 rpm. The resultant white powder was then pressed into pellets and annealed at 300°C for 5 hours under argon atmosphere.

XRD and NPD Measurement. The air-sensitive synthesized products were ground and sealed in a quartz capillary for subsequent powder XRD measurements. The tests were conducted on a PANalytical Empyrean X-ray diffractometer. Neutron powder diffraction data were collected at room temperature using the high-resolution powder diffractometer Echidna25 with neutrons of the wavelength 1.622 Å.[1] The air-sensitive samples were sealed in vanadium sample holders in Ar glove box. The GSAS II program was used for Rietveld refinement, with the Li_3ScCl_6 structure in the space group C2/m used as a starting model. The Cl occupancy on the 4i and 4j sites were fixed at their stoichiometric values. The atomic coordinates and atomic displacement parameters (U_{iso}) were restrained to be the same for the shared sites Sc1 and Zr1. The sum of occupancies was set to one for the shared sites [Occ.(Sc1) + Occ.(Zr1) = 1], and the atomic coordinates were restrained to be the same for Sc1 and Zr1 on the 2a site. All other parameters were subsequently refined.

NMR measurements. ^{7}Li NMR spectroscopy and ^{7}Li spin lattice relaxations (SLR) rates in experimental frame were measured on a Bruker AVANCE III 500 MHz NMR spectrometer (11.7 T) with a 7 mm high temperature MASCAT probe at 303 to 418 K temperature ranges with a spin rate of 4 kHz. The ^{7}Li SLR measurements were performed with the saturation recovery pulse program. ^{7}Li pulsed-field gradient (PFG) NMR were conducted on a Bruker AVANCE III 400 MHz NMR spectrometer (9.4 T) equipped a Diff50 gradient probe with a 5 mm ^{7}Li coil insert from 298 to 313 K. For ^{7}Li PFG NMR measurements, the bipolar-gradient pulse, stimulated-echo sequence (BPP-STE) were used [2] with δ = 1.5 ms and Δ = 30 ms. The ^{7}Li diffusion coefficient (D_{NMR}) were obtained by fitting the attenuation curves by Stejskal-Tanner equation.[3] The Larmor frequencies for ^{7}Li under the field of 11.7 T and 9.4 T are 194 and 155 MHz respectively. The ^{7}Li chemical shifts were referenced to LiCl (1 M a.q.) as 0 ppm.

Impedance Spectroscopy. The impedance spectroscopy (IS) measurements of $Li_{3-x}Sc_{1-x}Zr_xCl_6$ (x = 0, 0.25, 0.50, 0.625, 0.75, 1.0) were performed on a Zahner Im6ex in a frequency range between 8 MHz and 100 mHz with a 5mV potential amplitude. The annealed samples were first ground into powder and then loaded into an electrically insulating cylindrical cell. The powder was then cold-pressed by sandwiching between two stainless-steel electrodes under 300 MPa for the measurements.

The temperature dependence of the conductivity was measured at several specific temperatures ranging from 298 K to 333 K. For conductivity studies at each temperature, the samples were equilibrated for 1 h before the measurements. The temperature was controlled by placing the cells in a temperature chamber during measurement. The conductivity value is calculated by the standard formula, $\sigma = t/RA$, where t is the thickness of the pellet, A is the area of the pellet, and R is the resistance value obtained by fitting the impedance plots to the equivalent circuit model using the Zview program.

Linear Sweep Voltammetry measurement. The electrochemical stabilities of Li_3ScCl_6 and $Li_{2.375}Sc_{0.375}M_{0.625}Cl_6$ (M = Zr, Hf) were evaluated by linear sweep voltammetry (LSV) measurements. Firstly, 100 mg SE was pressed in a PEEK mold with a uniaxial pressure of 300 MPa. Subsequently, 20 mg composite cathode (prepared by mixing SE with carbon additive (VGCF) in a weight ratio of 70:30) was spread on one side of SE pellet, and pressed with a uniaxial pressure of 300 Mpa. Afterwards, 40 mg Li_6PS_5Cl was dispersed on the other side of the SE pellet, and pressed with the same pressure. Finally, Li-In alloy was attatched on the Li_6PS_5Cl layer, and the cell was sandwiched between two stainless-steel rods and sealed in a home-made cell. The LSV measurements were conducted by using VMP300 (Biologic) with a scan range from open-circuit voltage to 5 V or 0 V (vs. Li/Li^+) at a scan rate of 0.1mV s^{-1}.

Fabrication of All-solid-state Batteries. ASSBs using $Li_{2.375}Sc_{0.375}Zr_{0.625}Cl_6/Li_3ScCl_6$ solid electrolyte, $LiNi_{0.90}Co_{0.05}Mn_{0.05}O_2$ (Ni90)/$LiNi_{0.8}Co_{0.1}Mn_{0.1}O_2$ (Ni80) cathode and Li-In alloy anode were assembled in an argon-filled glovebox. The composite cathode mixtures were prepared by mixing cathode active material and solid electrolyte at a weight ratio of 8: 2. The Li-In alloy anode was prepared by pressing In foil onto the Li foil. ASSBs were assembled by the following procedures: First, ~40 mg Li_6PS_5Cl sulfide electrolyte powder was placed into a PEEK cyclinder and pressed at 3 tons for 1 min (10 mm diameter), after which ~60 mg $Li_{2.375}Sc_{0.375}Zr_{0.625}Cl_6/Li_3ScCl_6$ electrolyte powder was uniformly spread onto the surface of Li_6PS_5Cl sulfide electrolyte layer and pressed; Subsequently, ~6.0 mg composite cathode material was uniformly spread onto

the surface of $Li_{2.375}Sc_{0.375}Zr_{0.625}Cl_6$/$Li_3ScCl_6$ electrolyte layer and pressed at 3 tons for 1 min; Finally, Li-In foil was attached onto the other side of Li_6PS_5Cl sulfide electrolyte layer, and the cell was sandwiched between two stainless-steel rods and sealed in a home-made cell. Galvanostatic cycling test of the cells was conducted within the same voltage ranges at varied rates using LANHE (CT2001A, LAND Electronic Co. Ltd) battery test system. The cycling voltage range was set to 2.8-4.3 V *vs*. Li/Li^+ (or 2.2-3.7 V *vs*. Li-In) for ASSBs.

DFT Calculations. To identify the configurations with the lowest energy, we followed the procedure established in previous studies, and enumerated all symmetrically distinct configurations using electrostatic Ewald energy and density functional theory (DFT) calculations. All calculations throughout this study were performed utilizing the Vienna ab initio simulation package (VASP)[4] with the projector augmented-wave (PAW) method.[5] The generalized gradient approximation (GGA) function parameterized by Perdew-Burke-Ernzerhof (PBE)[6] was employed to describe the exchange-correlation potential. The cut-off energy was set to 520 eV. Geometry optimization was performed using the 2×1×2 supercells. Ionic relaxations were performed until the forces were converged to within 0.01 eV/Å and the convergence critetrion for the electronic self-consistency loop was set to 10^{-5} eV. A Γ-centered k-point mesh of 2×2×2 were used for the Brillouin integrations of the Li_3ScCl_6, $Li_{2.50}Sc_{0.50}Zr_{0.50}Cl_6$, $Li_{2.375}Sc_{0.375}Zr_{0.625}Cl_6$, $Li_{2.50}Sc_{0.50}Hf_{0.50}Cl_6$, and $Li_{2.375}Sc_{0.375}Hf_{0.625}Cl_6$.

The phase stability and electrochemical stability window of Li_3ScCl_6, $Li_{2.375}Sc_{0.375}Zr_{0.625}Cl_6$ and $Li_{2.375}Sc_{0.375}Hf_{0.625}Cl_6$ were screened by constructing the phase diagram and the grand potential phase diagram based on the data from Materials Project (MP). The phase stability was evaluated by calculating the energy above the convex hull (E_{hull}) against the competing stable phases in the MP. All the calculated reaction energies and voltages neglected the contribution of the PV terms and the entropy terms as in previous studies.[7] The phases with a positive E_{hull} values up to 25 meV/atom were considered as metastable phases, as they could be stabilized by entropic effects. Following previous studies,[8] the electrochemical stability window was

calculated using the grand potential phase diagram as a function of the chemical potential of Li

$$\mu_{\mathrm{Li}(\varphi)} = \mu_{\mathrm{Li},0} - e\varphi \qquad (1)$$

where $\mu_{\mathrm{Li},0}$ is the chemical potential of the Li metal, e is the elementary charge, and φ is the applied potential referenced to a Li metal anode. The Pymatgen code[9] was used to generate the grand phase diagram and determine the electrochemical stability window.

Bond Valence Site Energy (BVSE) Method. The probable Li^+-ion diffusion pathway and the corresponding migration energy barriers were predicted using the BVSE method as implemented in the SoftBV software.[10] Li site energies were calculated for a dense grid with a resolution of 0.1 Å using the Morse type interaction potential. The Li^+-ion migration path was identified based on the isosurface of the Li site energy.

AIMD simulations. *Ab initio* molecular dynamics (AIMD) simulations were carried out for the canonical (NVT) ensemble using a Nosé thermostat [11] at four elevated temperatures (650 K, 750 K, 850 K,and 950 K) in order to observe the diffusive behavior for the Li^+ ions over the time scale of our simulations. The volume and shape of the cell were fixed. The samples were heated up to the targeted temperature by velocity scaling over 5 *ps*, and then equilibrated at the desired temperature. The AIMD simulations were carried out for 200 *ps* at each temperature with a time step of 2 *fs*. To reduce the computational cost of the calculation, integration in reciprocal space was performed at the Γ-point only.

Correlation of Ion Dynamics. The van Hove correlation function[12] was calculated from the AIMD simulations. The van Hove correlation function can be split into the self-part G_s and the distinct-part G_d as follows:

$$G_s(r,t) = \frac{1}{4\pi r^2 N_\mathrm{d}} \left\langle \sum_{i=1}^{N_\mathrm{d}} \delta(r - |\vec{r}_i(t_0) - \vec{r}_i(t+t_0)|) \right\rangle_{t_0}$$

$$G_d(r,t) = \frac{1}{4\pi r^2 \rho N_\mathrm{d}} \left\langle \sum_{i\neq j}^{N_\mathrm{d}} \delta\left(r - \left|\vec{r}_i(t_0) - \vec{r}_j(t+t_0)\right|\right) \right\rangle_{t_0}$$

Here, δ is the Dirac delta function, and $\vec{r}_i(t)$ represents the position of the i^{th} particle at time t. N_d and r are the number of diffusing alkali ions in the unit cell and radial distance, respectively. The average number density serves as the normalization factor in G_d such that $G_d \rightarrow 1$ when $r \gg 1$. For a given r and t, $G_s(r, t)$ depicts the probability

that a particle will diffuse away from its initial positions by a distance r after a period t, whereas $G_d(r, t)$ describes the radial distribution of N-1 particles after a period t with respect to the initial reference particle.

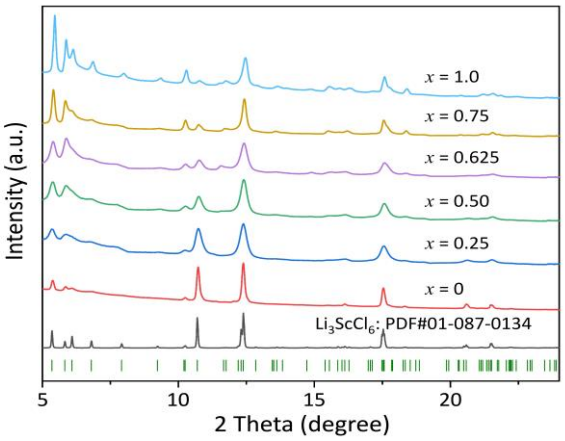

Figure S1. XRD patterns of $Li_{3-x}Sc_{1-x}Hf_xCl_6$ (x = 0, 0.25, 0.50, 0.625, 0.75, 1.0) collected with Ag Kα radiation.

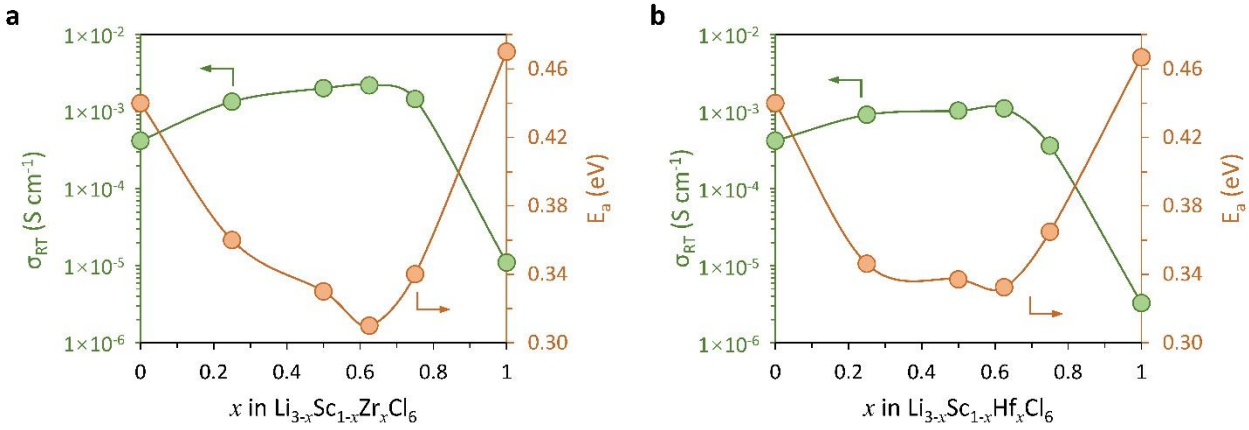

Figure S2. The room temperature ionic conductivities and activation energies of $Li_{3-x}Sc_{1-x}Hf_xCl_6$ (x = 0, 0.25, 0.50, 0.625, 0.75, 1.0).

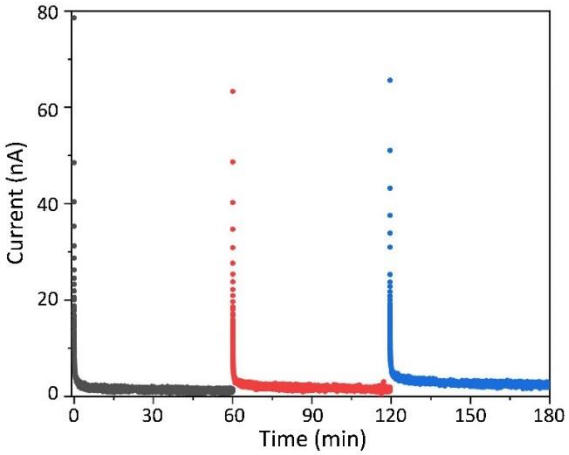

Figure S3. The electronic conductivity of $Li_{2.375}Sc_{0.375}Zr_{0.625}Cl_6$ measured by the DC polorization method at voltage of 100 mV (black curve), 200 mV (red curve) and 400 mV (blue curve).

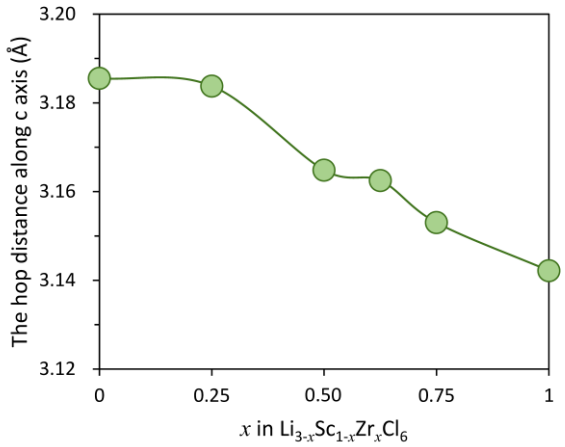

Figure S4. The Li^+-ion hop distance along the *c* axis in $Li_{3-x}Sc_{1-x}Zr_xCl_6$ (x = 0, 0.25, 0.625, 0.75, 1.0).

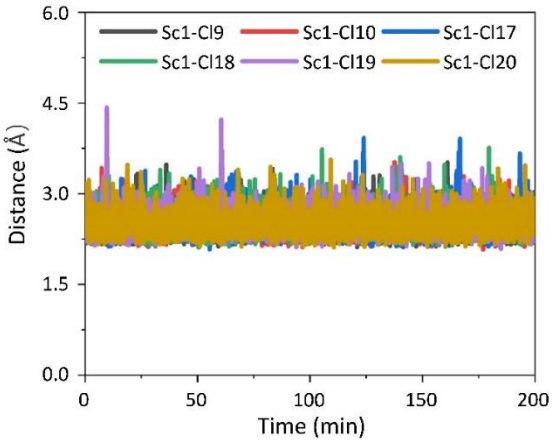

Figure S5. The bond length of Sc-Cl at 950 K in Li_3ScCl_6.

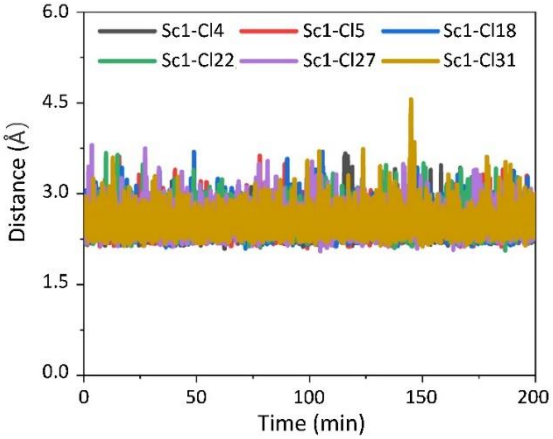

Figure S6. The bond length of Sc-Cl at 950 K in $Li_{2.375}Sc_{0.375}Zr_{0.625}Cl_6$.

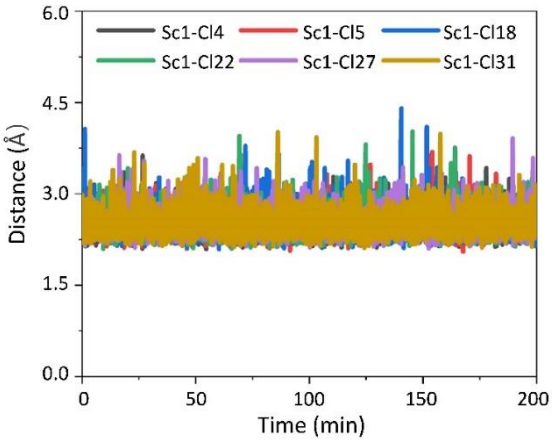

Figure S7. The bond length of Sc-Cl at 950 K in $Li_{2.375}Sc_{0.375}Hf_{0.625}Cl_6$.

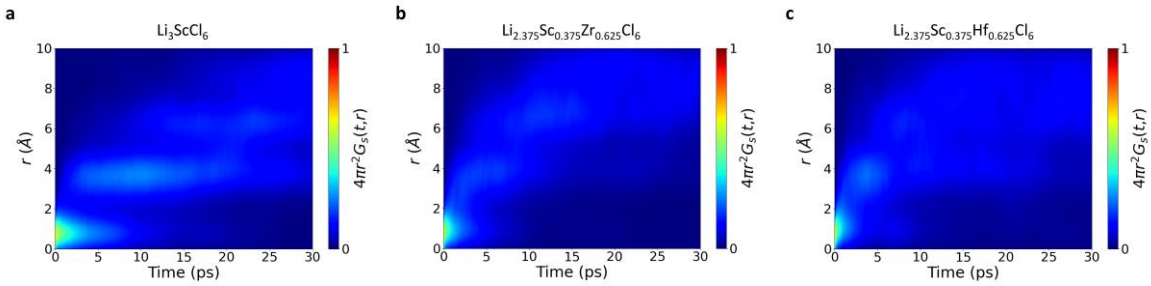

Figure S8. The self part of van Hove correlation function in (a) Li_3ScCl_6; (b) $Li_{2.375}Sc_{0.375}Zr_{0.625}Cl_6$; (c) $Li_{2.375}Sc_{0.375}Hf_{0.625}Cl_6$.

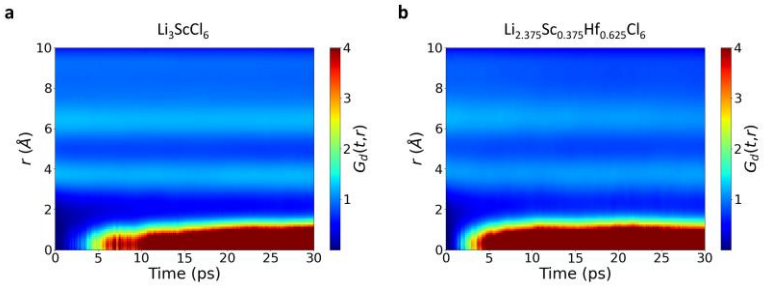

Figure S9. The distinctive part of van Hove correlation function in (a) Li_3ScCl_6; (b) $Li_{2.375}Sc_{0.375}Hf_{0.625}Cl_6$.

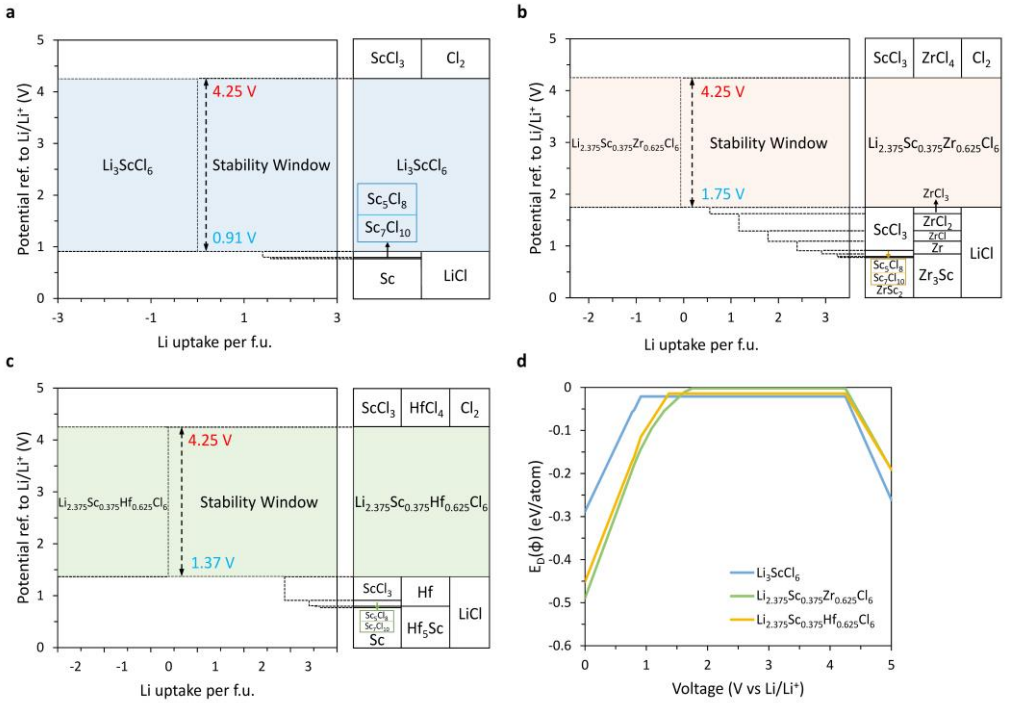

Figure S10. The thermodynamic equilibrium voltage profile of (a) Li_3ScCl_6, (b) $Li_{2.375}Sc_{0.375}Zr_{0.625}Cl_6$ and (c) $Li_{2.375}Sc_{0.375}Hf_{0.625}Cl_6$; (d) The phase equilibria of all the reaction stages based on DFT calculations. The thermodynamic intrinsic electrochemical windows for Li_3ScCl_6, $Li_{2.375}Sc_{0.375}Zr_{0.625}Cl_6$ and $Li_{2.375}Sc_{0.375}Zr_{0.625}Cl_6$ are 0.91 – 4.25 V, 1.75 – 4.25 V and 1.37 – 4.25 V (referenced to Li^+/Li), respectively.

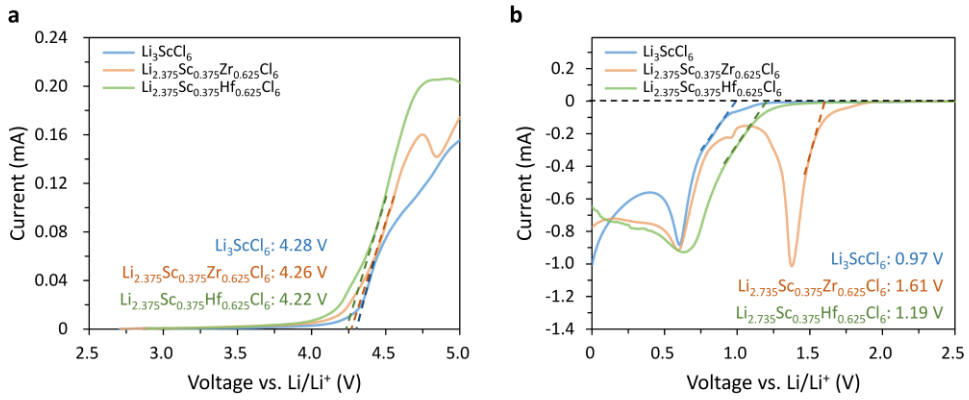

Figure S11. Linear sweep voltammetry curves of Li_3ScCl_6 and $Li_{2.375}Sc_{0.375}M_{0.625}Cl_6$ (M = Zr, Hf). The scan is performed from open circuit voltage to (a) 5 V and (b) 0 V (vs. Li/Li^+) at a rate of 0.1 mV s^{-1}. The resulting anodic limit for Li_3ScCl_6, $Li_{2.375}Sc_{0.375}Zr_{0.625}Cl_6$, and $Li_{2.375}Sc_{0.375}Hf_{0.625}Cl_6$ is 4.28, 4.26, and 4.22 V, respectively. And the cathodic limit for Li_3ScCl_6, $Li_{2.375}Sc_{0.375}Zr_{0.625}Cl_6$, and $Li_{2.375}Sc_{0.375}Hf_{0.625}Cl_6$ is 0.97, 1.61, and 1.19 V, respectively.

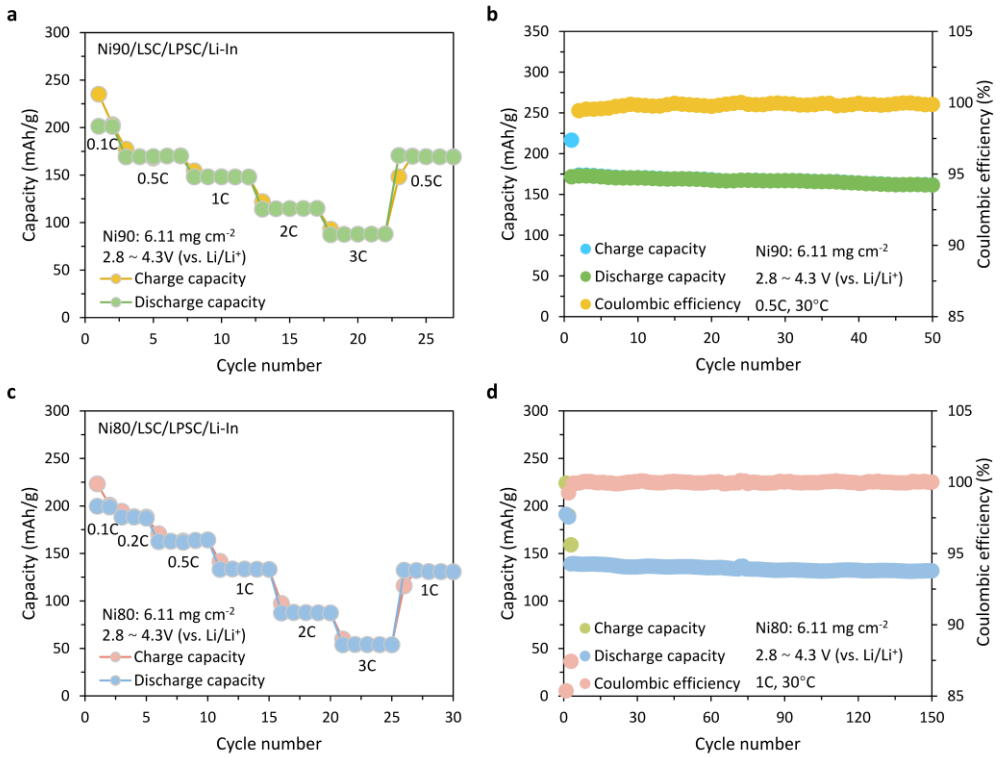

Figure S12. (a) The rate performance of Ni90/LSC/LPSC/Li-In solid-state battery cycled at different rates (0.1C, 0.5C, 1C, 2C, and 3C); (b) The cycling performance of Ni90/LSC/LPSC/Li-In solid-state battery under 0.5C; (c) The rate performance of Ni80/LSC/LPSC/Li-In solid-state battery cycled at different rates (0.1C, 0.2C, 0.5C, 1C, 2C, and 3C); (d) The cycling performance of Ni80/LSC/LPSC/Li-In solid-state battery; The cell was charged/discharged at 0.1C during the first two cycles and subsequently at 1C for the rest

Table S1. Structural parameters for monoclinic Li_3ScCl_6 based on the NPD data collected at room temperature. Space group *C*2/*m* (No 12). Cell parameters a = 6.3876(4) Å, b = 11.0763(6) Å, c = 6.3630(4) Å, β = 109.394(7)°, volume = 424.64(4) Å^3.

Atom	Wyckoff site	*x*	*y*	*z*	Occupancy	U_{iso} (Å^2)
Li1	4g	0	0.844(6)	0	0.6349(4)	0.104(6)
Li2	4h	0.0	0.195(5)	0.5	0.5399(5)	0.104(6)
Li3	2d	0.5	0	0.5	0.6511(8)	0.104(6)
Sc1	2a	0	0	0	1	0.0322(6)
Cl1	4i	0.7487(10)	0	0.2391(7)	1	0.0259(5)
Cl2	8j	0.2360(6)	0.83848(30)	0.2336(4)	1	0.02289(24)
Agreement factors: R_p = 3.61%, R_{wp} = 4.68%, GoF = 4.836						

Table S2. Structural parameters for monoclinic $Li_{2.75}Sc_{0.75}Zr_{0.25}Cl_6$ based on the NPD data collected at room temperature. Space group *C*2/*m* (No 12). Cell parameters a = 6.3912(10) Å, b = 11.0891(19) Å, c = 6.3544(9) Å, β = 109.336(12)°, volume = 424.94(8) Å^3.

Atom	Wyckoff site	*x*	*y*	*z*	Occupancy	U_{iso} (Å^2)
Li1	4g	0.5	0.834(7)	0	0.659(31)	0.103(9)
Li2	4h	0	0.183(9)	0.5	0.44(4)	0.103(9)
Li3	2d	0.5	0	0.5	0.57(7)	0.103(9)
Sc1	2a	0	0	0	0.75	0.0309(12)
Zr1	2a	0	0	0	0.25	0.0309(12)
Cl1	4i	0.7512(12)	0	0.2392(9)	1	0.0288(11)
Cl2	8j	0.2364(9)	0.8389(4)	0.2333(5)	1	0.0240(6)
Agreement factors: R_p =2.83%, R_{wp} = 3.71%, GoF = 3.203						

Table S3. Structural parameters for monoclinic $Li_{2.375}Sc_{0.375}Zr_{0.625}Cl_6$ based on the NPD data collected at room temperature. Space group *C*2/*m* (No 12). Cell parameters a = 6.3993(13) Å, b = 11.1048(23) Å, c = 6.3323(13) Å, β = 109.291(14)°, volume = 424.73(15) Å^3.

Atom	Wyckoff site	*x*	*y*	*z*	Occupancy	U_{iso} (Å^2)
Li1	4g	0.5	0.856(5)	0	0.589(33)	0.022(7)
Li2	4h	0	0.187(7)	0.5	0.38(5)	0.022(7)
Li3	2d	0.5	0	0.5	0.44(8)	0.022(7)
Sc1	2a	0	0	0	0.375	0.0198(25)
Zr1	2a	0	0	0	0.625	0.0198(25)
Cl1	4i	0.7540(18)	0	0.2420(11)	1	0.0288(16)
Cl2	8j	0.2405(14)	0.8402(6)	0.2341(7)	1	0.0268(9)
Agreement factors: R_p = 2.91%, R_{wp} = 3.87%, GoF = 3.825						

Table S4. Structural parameters for monoclinic $Li_{2.25}Sc_{0.25}Zr_{0.75}Cl_6$ based on the NPD data collected at room temperature. Space group *C*2/*m* (No 12). Cell parameters a = 6.4010(10) Å, b = 11.0940(15) Å, c = 6.3228(7) Å, β = 109.490(9)°, volume = 423.28(9) Å^3.

Atom	Wyckoff site	*x*	*y*	*z*	Occupancy	U_{iso} (Å^2)
Li1	4g	0.5	0.841(7)	0	0.58(4)	0.033(9)
Li2	4h	0	0.204(8)	0.5	0.35(6)	0.033(9)
Li3	2d	0.5	0.0	0.5	0.42(8)	0.033(9)
Sc1	2a	0	0.0	0	0.25	0.0207(25)
Zr1	2a	0	0.0	0	0.75	0.0207(25)
Cl1	4i	0.7538(18)	0	0.2411(12)	1	0.0293(17)
Cl2	8j	0.2389(13)	0.8403(5)	0.2346(7)	1	0.0248(9)
Agreement factors: R_p = 3.58%, R_{wp} = 4.66%, GoF = 4.163						

Table S5. Structural parameters for monoclinic Li_3ScCl_6 based on the XRD data collected at room temperature. Space group *C*2/*m* (No 12). Cell parameters *a* = 6.3752(20) Å, *b* = 11.0527(4) Å, *c* = 6.3711(21) Å, *β* = 109.264(6)°, volume = 423.791(28) Å^3.

Atom	Wyckoff site	*x*	*y*	*z*	Occupancy	U_{iso} (Å^2)
Li1	4g	0.5	0.8412(28)	0	0.68(3)	0.029(4)
Li2	4h	0	0.2022(22)	0.5	0.57(4)	0.029(4)
Li3	2d	0.5	0.0	0.5	0.50(7)	0.029(4)
Sc1	2a	0	0.0	0	1	0.0266(10)
Cl1	4i	0.7471(6)	0	0.2396(4)	1	0.03002(29)
Cl2	8j	0.2378(4)	0.83619(30)	0.23435(31)	1	0.03002(29)

Table S6. Structural parameters for monoclinic $Li_{2.75}Sc_{0.75}Zr_{0.25}Cl_6$ based on the XRD data collected at room temperature. Space group *C*2/*m* (No 12). Cell parameters *a* = 6.3772(11) Å, *b* = 11.05825(30) Å, *c* = 6.3676(13) Å, *β* = 109.5398(29)°, volume = 423.187(30) Å^3.

Atom	Wyckoff site	*x*	*y*	*z*	Occupancy	U_{iso} (Å^2)
Li1	4g	0.5	0.8274(19)	0	0.666(23)	0.018(4)
Li2	4h	0	0.1976(22)	0.5	0.353(31)	0.018(4)
Li3	2d	0.5	0.0	0.5	0.71(5)	0.018(4)
Sc1	2a	0	0.0	0	0.75	0.0237(7)
Zr1	2a	0	0.0	0	0.25	0.0237(7)
Cl1	4i	0.7503(5)	0	0.2377(4)	1	0.0291(4)
Cl2	8j	0.23675(26)	0.83855(16)	0.23376(31)	1	0.0291(4)

Table S7. Structural parameters for monoclinic $Li_{2.50}Sc_{0.50}Zr_{0.50}Cl_6$ based on the XRD data collected at room temperature. Space group *C*2/*m* (No 12). Cell parameters *a* = 6.3808(23) Å, *b* = 11.0749(7) Å, *c* = 6.3297(24) Å, *β* = 109.520(6)°, volume = 421.59(5) Å^3.

Atom	Wyckoff site	*x*	*y*	*z*	Occupancy	U_{iso} (Å^2)
Li1	4g	0.5	0.842(22)	0	0.58(4)	0.042(6)
Li2	4h	0	0.212(27)	0.5	0.52(15)	0.042(6)
Li3	2d	0.5	0.0	0.5	0.40(26)	0.042(6)
Sc1	2a	0	0.0	0	0.5	0.0204(4)
Zr1	2a	0	0.0	0	0.5	0.0204(4)
Cl1	4i	0.7494(5)	0	0.2401(7)	1	0.03000(29)
Cl2	8j	0.2362(3)	0.83835(20)	0.2335(4)	1	0.03000(29)

Table S8. Structural parameters for monoclinic $Li_{2.375}Sc_{0.375}Zr_{0.625}Cl_6$ based on the XRD data collected at room temperature. Space group *C*2/*m* (No 12). Cell parameters a = 6.3814(21) Å, b = 11.0808(6) Å, c = 6.3251(23) Å, β = 109.796(6)°, volume = 420.82(3) Å^3.

Atom	Wyckoff site	*x*	*y*	*z*	Occupancy	U_{iso} (Å^2)
Li1	4g	0.5	0.8622(28)	0	0.585(23)	0.047(5)
Li2	4h	0	0.192(4)	0.5	0.389(27)	0.047(5)
Li3	2d	0.5	0.0	0.5	0.43(5)	0.047(5)
Sc1	2a	0	0.0	0	0.375	0.0202(3)
Zr1	2a	0	0.0	0	0.625	0.0202(3)
Cl1	4i	0.75348(27)	0	0.2427(4)	1	0.0289(3)
Cl2	8j	0.24034(22)	0.84037(15)	0.23348(30)	1	0.0289(3)

Table S9. Structural parameters for monoclinic $Li_{2.25}Sc_{0.25}Zr_{0.75}Cl_6$ based on the XRD data collected at room temperature. Space group *C*2/*m* (No 12). Cell parameters a = 6.3819(17) Å, b = 11.0720(5) Å, c = 6.3060(17) Å, β = 109.362(5)°, volume = 420.388(22) Å^3.

Atom	Wyckoff site	*x*	*y*	*z*	Occupancy	U_{iso} (Å^2)
Li1	4g	0.5	0.837(4)	0	0.589(27)	0.052(7)
Li2	4h	0	0.207(7)	0.5	0.27(4)	0.052(7)
Li3	2d	0.5	0.0	0.5	0.54(7)	0.052(7)
Sc1	2a	0	0.0	0	0.25	0.0204(3)
Zr1	2a	0	0.0	0	0.75	0.0204(3)
Cl1	4i	0.7545(6)	0	0.2410(4)	1	0.03004(29)
Cl2	8j	0.2387(3)	0.84030(15)	0.23449(31)	1	0.03004(29)

Table S10. Structural parameters for monoclinic Li_2ZrCl_6 based on the XRD data collected at room temperature. Space group *C*2/*m* (No 12). Cell parameters a = 6.3870(18) Å, b = 11.0574(4) Å, c = 6.2934(18) Å, β = 109.678(5)°, volume = 418.505(29) Å^3.

Atom	Wyckoff site	*x*	*y*	*z*	Occupancy	U_{iso} (Å^2)
Li1	4g	0.5	0.8387(28)	0	0.48(4)	0.073(11)
Li2	4h	0	0.212(15)	0.5	0.13(4)	0.073(11)
Li3	2d	0.5	0.0	0.5	0.78(8)	0.073(11)
Zr1	2a	0	0.0	0	1	0.0207(25)
Cl1	4i	0.75482(29)	0	0.2419(6)	1	0.0318(4)
Cl2	8j	0.23812(20)	0.84031(9)	0.2337(3)	1	0.0318(4)

References

(1) Avdeev, M.; Hester, J. R. ECHIDNA: a decade of high-resolution neutron powder diffraction at OPAL. *J. Appl. Crystallogr.* **2018**, *51*, 1597-1604.

(2) Wu, D.; Chen, A.; Johnson, C. S. An improved diffusion-ordered spectroscopy experiment incorporating bipolar-gradient pulses. *J. Magn. Reson.* **1995**, *115*, 260-264.

(3) Stejskal, E. O.; Tanner, J. E. Spin diffusion measurements: spin echoes in the presence of a time-dependent field gradient. *J. Chem. Phys.* **1965**, *42*, 288-292.

(4) Kresse, G.; Furthmüller, J. Efficiency of ab-initio total energy calculations for metals and semiconductors using a plane-wave basis set. *Comput. Mater. Sci.* **1996**, *6*, 15-50.

(5) Blöchl, P. E. Projector augmented-wave method. *Phys. Rev. B* **1994**, *50*, 17953.

(6)Perdew, J. P.; Burke, K.; Ernzerhof, M. Generalized gradient approximation made simple. *Phys. Rev. Lett.* **1996**, *77*, 3865.

(7) Ong, S. P.; Wang, L.; Kang, B.; Ceder, G. Li-Fe-P-O_2 phase diagram from first principles calculations. *Chem. Mater.* **2008**, *20*, 1798-1807.

(8) Zhu, Y.; He, X.; Mo, Y. Origin of outstanding stability in the lithium solid electrolyte materials: insights from thermodynamic analyses based on first-principles calculations. *ACS Appl. Mater. Interfaces* **2015**, *7*, 23685-23693.

(9) Ong, S. P.; Richards, W. D.; Jain, A.; Hautier, G.; Kocher, M.; Cholia, S.; Gunter, D.; Chevrier, V. L.; Persson, K. A.; Ceder, G. Python Materials Genomics (pymatgen): A robust, open-source python library for materials analysis. *Comput. Mater. Sci.* **2013**, *68*, 314-319.

(10) Chen, H.; Wong, L. L.; Adams, S. SoftBV-a software tool for screening the materials genome of inorganic fast ion conductors. *Acta Crystallogr. B* **2019**, *75*, 18-33.

(11) Martyna, G. J.; Klein, M. L.; Tuckerman, M. Nosé–Hoover chains: the canonical ensemble via continuous dynamics. *J. Chem. Phys.* **1992**, *97*, 2635-2643.

(12) Van Hove, L. Correlations in space and time and Born approximation scattering in systems of interacting particles. *Phys. Rev.* **1954**, *95*, 249.